



**HAL**  
open science

## Separation of kinetic rate orders in extreme ultraviolet transient grating spectroscopy

Hugo Marroux, Serhii Polishchuk, Oliviero Cannelli, Rebecca Ingle, Giulia Mancini, Camila Bacellar, Michele Puppini, Romain Geneaux, Gregor Knopp, Laura Foglia, et al.

### ► To cite this version:

Hugo Marroux, Serhii Polishchuk, Oliviero Cannelli, Rebecca Ingle, Giulia Mancini, et al.. Separation of kinetic rate orders in extreme ultraviolet transient grating spectroscopy. *Journal of Physics B: Atomic, Molecular and Optical Physics*, 2024, 57 (11), pp.115401. 10.1088/1361-6455/ad421f. cea-04888999

**HAL Id: cea-04888999**

<https://cea.hal.science/cea-04888999v1>

Submitted on 15 Jan 2025

**HAL** is a multi-disciplinary open access archive for the deposit and dissemination of scientific research documents, whether they are published or not. The documents may come from teaching and research institutions in France or abroad, or from public or private research centers.

L'archive ouverte pluridisciplinaire **HAL**, est destinée au dépôt et à la diffusion de documents scientifiques de niveau recherche, publiés ou non, émanant des établissements d'enseignement et de recherche français ou étrangers, des laboratoires publics ou privés.



Distributed under a Creative Commons Attribution 4.0 International License

# Separation of kinetic rate orders in extreme ultraviolet transient grating spectroscopy

Hugo J B Marroux<sup>1,2,\*</sup>, Serhii Polishchuk<sup>1</sup>, Oliviero Cannelli<sup>1,3</sup> , Rebecca A Ingle<sup>1,4</sup> , Giulia F Mancini<sup>1,5</sup>, Camila Bacellar<sup>1,6</sup>, Michele Puppini<sup>1</sup>, Romain Geneaux<sup>2</sup> , Gregor Knopp<sup>6</sup>, Laura Foglia<sup>7</sup>, Emanuele Pedersoli<sup>7</sup> , Flavio Capotondi<sup>7</sup>, Ivaylo Petrov Nikolov<sup>7</sup>, Filippo Bencivenga<sup>7</sup> , Riccardo Mincigrucci<sup>7</sup>, Claudio Masciovecchio<sup>7</sup> and Majed Chergui<sup>1,7,\*</sup> 

<sup>1</sup> Lausanne Centre for Ultrafast Science (LACUS), ISIC, École Polytechnique Fédérale de Lausanne (EPFL), CH-1015 Lausanne, Switzerland

<sup>2</sup> Université Paris-Saclay, CEA, LIDYL, 91191 Gif-sur-Yvette, France

<sup>3</sup> Centre for Free-electron Laser Science, Deutsches Elektronen-Synchrotron, Notkestr. 85, 22607 Hamburg, Germany

<sup>4</sup> Department of Chemistry, University College London, 20 Gordon Street, London WC1H 0AJ, United Kingdom

<sup>5</sup> Laboratory for Ultrafast X-ray and Electron Microscopy (LUXEM), Department of Physics, University of Pavia, I-27100 Pavia, Italy

<sup>6</sup> SwissFEL, Paul-Scherrer-Institut (PSI), 5232 Villigen PSI, Switzerland

<sup>7</sup> Elettra-Sincrotrone Trieste S.C.p.A., S.S. 14 km 163, 5 in Area Science Park, I-34012 Basovizza, Trieste, Italy

E-mail: [hugo.marroux@cea.fr](mailto:hugo.marroux@cea.fr), [majed.chergui@epfl.ch](mailto:majed.chergui@epfl.ch) and [majed.chergui@elettra.eu](mailto:majed.chergui@elettra.eu)

Received 12 January 2024, revised 30 March 2024

Accepted for publication 23 April 2024

Published 7 May 2024



## Abstract

We present an extreme ultraviolet (EUV) transient grating (TG) experiment of the spinel  $\text{Co}_3\text{O}_4$  compound using tuneable incident energies across the Co  $M_{2,3}$ -edge and a 395 nm probe pulse, detecting both the first and the second diffraction orders (SDOs). While the first diffraction order shows a monotonous behavior as a function of time, with a sharp response at  $t = 0$ , followed by a weak sub-picosecond component and a nearly constant signal thereafter, the time dependence of SDO varies dramatically with the incident energy as it is tuned across the Co M-edge, with the appearance of a component at  $t > 1$  ps that grows with increasing energy. The results are rationalized in terms of the deviations of the initial grating from sinusoidal to non-sinusoidal, namely a flattening of the grating pattern, that introduces new Fourier components. These deviations are due to higher order, three-body terms in the population

\* Authors to whom any correspondence should be addressed.



Original content from this work may be used under the terms of the [Creative Commons Attribution 4.0 licence](https://creativecommons.org/licenses/by/4.0/). Any further distribution of this work must maintain attribution to the author(s) and the title of the work, journal citation and DOI.

relaxation kinetics. The present results highlight the use of the SDO response in EUV TG as a tool to identify higher order terms in the population kinetics.

Supplementary material for this article is available [online](#)

Keywords: electron-hole recombination, transient gratings, spinel cobalt oxide, ultrafast, extreme ultraviolet

## 1. Introduction

In solids, photoexcitation of charge carriers in solid materials, e.g. semiconductors, gives rise to a series of processes, which include electron–electron, electron–phonon and phonon–phonon scattering, polaron formation, and electron-hole recombination. The latter can be described by a superposition of first-, and higher-order recombination processes [1, 2]. One of the key efforts in studies of charge carrier dynamics in solids is to disentangle these various contributions and separate the different order terms. This is in particular the case for the electron-hole recombination, whose regime strongly depends on the density of charge carriers. The separation of the various order terms in the recombination kinetics of a photoexcited system is usually dealt with by conventional time-resolved spectroscopies (e.g. transient absorption, fluorescence up-conversion, etc.), but this is complicated, as each term contributes to the population of the same species.

Transient grating (TG) spectroscopy is a tool potentially capable of separating the contributions of high and lower kinetic terms. In TG experiments, two spatially and temporally overlapped identical laser beams with wavelength  $\lambda_{\text{ex}}$  are crossed at an angle  $2\theta$  on the sample creating an excitation grating by interference onto which a third, time-delayed probe pulse scatters (figure 1) [3]. The interference patterns by the two laser beams, yields a spatially varying distribution of excitation,  $\frac{1 - \cos\left(\frac{2\pi x}{L_{\text{TG}}}\right)}{2}$  where  $L_{\text{TG}} = \lambda_{\text{ex}}/(2\sin\theta)$  is the grating period. TG spectroscopy follows the same non-linear interaction sequence as transient absorption and it therefore yields the same spectroscopic content, however with the advantage that the signal is detected in a background-free region, and that the spectral information is combined with a spatial one due to the periodic pattern of excitation.

Optical-domain TG spectroscopy is commonly used to study energy, charge and heat transport in gases, liquids and solids [3–5], and has served as a stepping stone for the development of ultrafast multi-dimensional spectroscopy [6]. However, only a handful of studies have pointed to the fact that TG spectroscopy can reveal higher orders of the relaxation kinetics by detecting the time dependence of higher diffraction orders. These experiments were conducted on the picosecond timescale, revealing exciton–exciton annihilation in organic dyes [7, 8] and in the microsecond timescale, investigating the rates of bimolecular reactions [9]. However, optical domain TG experiments lack element-selectivity.

In this respect, there have been over the past few years, major achievements aimed at extending TG experiments to the short-wavelengths in the extreme ultraviolet (EUV) and hard x-ray ranges [10, 11]. In addition to providing element-selectivity via the core-transitions, the EUV/x-ray wavelengths allow for smaller grating periods, down to the nm-scale and, as a corollary, for larger momentum transfers [11]. Short-wavelength TG was first demonstrated in the EUV using an optical probe pulse [12] and later, using an EUV probe pulse [13]. These initial demonstrations led to a flurry of EUV TG studies on the generation of coherent acoustic and optical phonons [14, 15], the element-specificity of the EUV-generated resonant TG [16], and on the generation, control and probing of magnetic patterns [17]. Recently, core-level TG spectroscopy has been extended into the hard x-ray range and the created TG was probed by an optical pulse [18]. It should be stressed that the all-EUV TG study on magnetic gratings in a GdFe alloy by Yao *et al* [19] reported both the first diffraction order (FDO) and second diffraction order (SDO) traces, allowing them to demonstrate ultrafast all-optical switching on the nanometer length scale.

Core-level excitation of materials releases a cascade of electrons within the first instants of the interaction ( $<100$  fs), either via fast Auger decay of the atomic core-excitation or via secondary impact ionization of high kinetic energy electrons. This inner-valence or core-excitation represents a significantly different type of excitation to a valence one, as the released electrons then undergo a rich variety of cooling, diffusion and recombination processes. Ultimately in solids, inter band-gap electron-hole recombination will occur, which is described by the following equation:

$$\frac{\partial N(x,t)}{\partial t} = D \frac{\partial^2 N}{\partial x^2} - k_1 N - k_2 N^2 - k_3 N^3 \quad (1)$$

with  $N(x,t)$  being the spatio-temporal distribution of carriers,  $D$  the diffusion coefficient,  $k_1$ ,  $k_2$  and  $k_3$  the single, two- or three-body bulk recombination rates. The three-body process is represented by the interband Auger recombination (IAR, different to the intra-atomic one invoked above), in which an electron recombines with a hole while exciting a third carrier to a higher-energy state. This can be viewed as two electrons colliding in the vicinity of a hole, resulting in a radiationless e–h recombination event. Here, we show that by EUV-TG spectroscopy on multiple orders of diffraction in the case of spinel  $\text{Co}_3\text{O}_4$ , we can identify when the population kinetics

are dominated by one or the other order term of equation (1), depending on the initial conditions of charge carrier densities.

The choice of  $\text{Co}_3\text{O}_4$  is motivated by its remarkable photophysical properties. It is composed of  $\text{O}^{2-}$  anions forming a face-centred cubic lattice where the  $\text{Co}^{2+}$  and  $\text{Co}^{3+}$  ions are, respectively, located in tetrahedral and octahedral sites with a 1:2 stoichiometry. The local coordination of the metallic centers determines a high spin ( $S = 3/2$ ,  ${}^4\text{A}_2$  state) electronic configuration for the tetrahedrally-coordinated  $d^7$   $\text{Co}^{2+}$  ions and a low spin ( $S = 0$ ,  ${}^1\text{A}_1$  state) configuration for the octahedrally-coordinated  $d^6$   $\text{Co}^{3+}$  ones. This confers the system a peculiar optical absorption spectrum [10], with Mott–Hubbard and charge transfer gaps that are close in energy, and involves excitations to metal-centred (d–d, 0.5–1 eV), metal-to-metal charge transfer 1.3–2 eV and ligand-to-metal charge transfer  $>2$  eV states. The photophysics of the system has been investigated by ultrafast methods, such as optical-pump/optical-probe techniques [20], optical pump/EUV probe at the Co M-edges [21] and O  $L_1$  edge [22], and optical pump/near-IR probe spectroscopies [23]. These studies show that by the first ps, the excited population settles in the long-lived (up to nanoseconds), presumably, the lowest lying d–d states.

We applied EUV-TG spectroscopy to the case of the electronic relaxation of a thin spinel  $\text{Co}_3\text{O}_4$  film excited at the cobalt (Co)  $M_{2,3}$ -edges in the 57–67 eV region using the FERMI free electron laser (FEL) [24, 25]. The importance of the different kinetic rate orders as a function of the initial excited carrier density is evidenced via the tuning of the FEL photon energy ( $E_{\text{exc}}$ ) across the Co  $M_{2,3}$  edge at constant power. At lower excitation densities, i.e. when the  $E_{\text{exc}}$  is below the Co edges, the time evolution of the FDO and SDO shows that the photoinduced grating is only marginally distorted by the high order kinetic terms of equation (1). As  $E_{\text{exc}}$  is scanned across the Co  $M_{2,3}$  edge, the initial excitation density is increased from  $2.5 \times 10^{20} \text{ cm}^{-3}$  to  $6.4 \times 10^{20} \text{ cm}^{-3}$ , regardless of the mechanism that generates it, and phenomena described by high order terms of equation (1) start to influence the kinetics. The dominant mechanisms at the highest carrier densities are attributed to the three-body process of IAR.

## 2. Results

The geometry of the TG experiment is displayed in figure 1 and detailed in the methods section. Briefly, the two energy-tunable EUV pulses are incident at an angle of  $2\theta = 2.7^\circ$  on the sample, generating a cosine excitation grating with  $L_{\text{TG}}$  ranging from 478 to 376 nm depending on  $E_{\text{exc}}$ . The evolution of the grating is followed by scattering a 395 nm pulse incident at  $45^\circ$  on the sample, which is time-delayed with respect to the EUV excitation pulses. The FDO and SDO can be followed by rotating an in-vacuum camera at the phase matched directions.

Figure 2 shows the time evolution of the spatially integrated FDO and SDO traces for different  $E_{\text{exc}}$ . The traces are the average of three consecutive scans and the error bars represent one sigma of the FEL shot-to-shot intensity fluctuation as it is the main source of noise in the measurement. The FDO

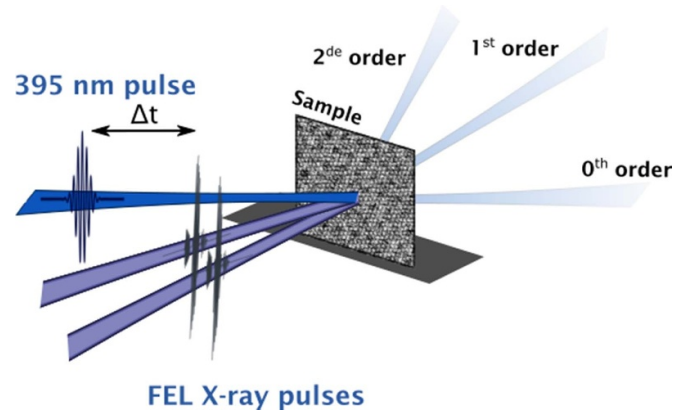


**Figure 1.** Experimental layout for EUV transient grating spectroscopy in the first and second diffraction orders.

traces (figure 2(a)) are characterized by a sharp response at  $t = 0$ , followed by a slower decay (in the order of hundreds of fs), and then a flat signal that further decays on the nanosecond timescale due to charge carrier diffusion and recombination. The long-time behavior of the FDO at 59 eV is shown in figure S3, and it confirms the long-time signal reported in pump-probe studies [20–24], pointing to the electronic origin of this signal. Most important is that in figure 2(a), overall only minor changes occur in the profile of the FDO traces as a function of  $E_{\text{exc}}$ . The FDO profiles follow a similar trend as the ones obtained by Bohinc *et al* at the Si  $L_{2,3}$  edge of silicon nitride ( $\text{Si}_3\text{N}_4$ ) [16]. However, contrary to this report where the decay time was seen to dramatically shorten upon crossing into the Si  $L_{2,3}$  edge, in our case they lengthen as we scan the incident energy across the Co M-edges. This warrants a more detailed discussion, which we will present in a separate article, while the focus here is on comparison of FDO and SDO traces.

The SDO temporal traces (figure 2(b)) show a quite different behaviour, with large variations as a function of  $E_{\text{exc}}$ . Below the Co  $M_{2,3}$  edge, e.g.  $E_{\text{exc}} = 57$  eV, the SDO trace displays a temporal evolution similar to the FDO traces, i.e. an intense time zero signal followed by a fast and a slow component, although with relative different weights compared to the FDO traces. One can also distinguish a weak broad feature peaking near 3 ps. When the initial carrier density is increased by tuning  $E_{\text{exc}}$  across the Co  $M_{2,3}$  edge, the fast component is still present but the signal increases at later times, becoming even larger than the  $t = 0$  signal. The data are quite noisy but the trace at  $E_{\text{exc}} = 64$  eV shows a clear maximum around 3 ps. When comparing the relative intensities of the  $t = 0$  peak to the signal at 3–4 ps, we see that for the SDO signal there is a four-fold increase in intensity upon scanning  $E_{\text{exc}}$  across the Co M-edge, while on the FDO traces the variation is negligible. Furthermore, there seems to be a trend for the maximum signal to shift to earlier times with increasing  $E_{\text{exc}}$ , at least if one compares the 57, 64 and 67 eV traces. However, the data are overall quite noisy, and further measurements would be needed to be more affirmative.

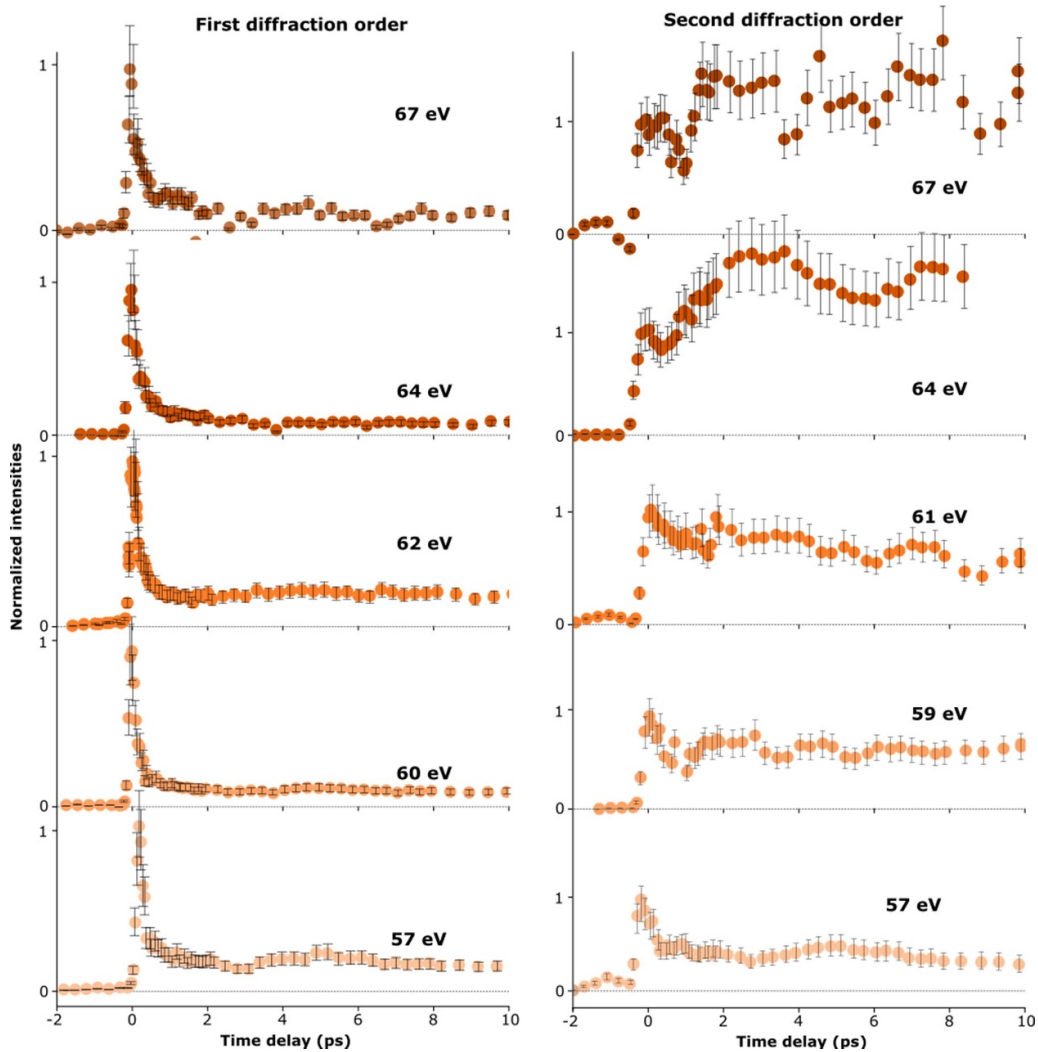


**Figure 2.** Time evolution of the first (FDO) and second diffraction order (SDO) of a 395 nm probe pulse on the EUV transient grating created on  $\text{Co}_3\text{O}_4$  with the FEL pulses tuned at the indicated incident energies. The FDO time traces display minor variations with incident photon energy, while the SDO traces change dramatically and reveal a delayed signal increase as the photon energy is tuned across the Co  $M_{2,3}$  edge. All trace intensities are scaled to the time zero signal and the error bars correspond to one sigma of the FEL shot-to-shot intensity fluctuations.

These trends bear remarkable resemblances with the optical TG traces reported by Samoc and Prasad for molecular crystals [7]. In particular, they predicted by theory that for the case of bimolecular decay kinetics, the time lag between the maxima of the first-order and second-order diffraction signals should decrease as the input power increases. Here, as we tune the incident photon energy across the  $M_{2,3}$ -edges of Co, we effectively increase the carrier density by a factor of  $\sim 2.5$  (see above), we can rule out effects due to changes in  $L_{\text{TG}}$  as the latter is modified by  $\sim 100$  nm between 57 and 64 eV, while the signal exhibits a 4-fold variation in intensity for the 395 nm probe. The  $\sim 100$  nm change in the line spacing will increase the diffraction intensity by a factor of 1.6 between the 57 and 64 eV traces. Unfortunately, due to experimental constraints the time traces at the different photon energies cannot be compared in intensity directly so the data analysis is done on normalized amplitudes.

### 3. Discussion

In TG experiments, the spatial profile of the initial electronic excitation grating follows the EUV beam interference pattern. If the EUV energy is tuned above the core-ionization threshold, the created core-holes are refilled by decay of electrons from higher lying energy levels. For cobalt, the core-hole decay occurs in less than 5 fs, i.e. well within the EUV pulse duration (estimated to be  $\sim 50$  fs) [26]. The released electrons are thermalized via electron-electron scattering whose timing strongly depends on the electron energy and the charge carrier density [27]. At later times, electron-phonon scattering sets in causing the generation of a lattice temperature grating, acoustic and optical phonons.

While for optical and UV excitations the electronic thermalization time is considered to be in the range of tens to hundreds of fs depending on the material and excitation conditions [20, 28, 29], in the case of electrons with kinetic



energies much higher than the band-gap energy it is considerably faster ( $<25$  fs), due to impact ionization [30, 31]. The increase of charge carrier density through impact ionization can be an order of magnitude higher than the initial charge carrier density in the EUV range, depending on the density of states and the ratio between  $E_{\text{exc}}$  and the bandgap energy. On the ps timescale, charge carrier dynamics can be driven by electron-hole recombination, IAR, and carrier diffusion [1, 2, 16]. For high charge carrier densities, IAR becomes dominant on the short time scale due to its third order kinetic equation [29, 32–34].

An accurate reporting of the time constants of these kinetics using TG is generally difficult. The intensity of a diffraction order depends not only on the population of photoproducts but also on the Fourier components of the grating. In the simplest case, i.e. with first order kinetic equations [9] and non-saturated absorption [7], the time evolution of the FDO signal is sufficient to determine the population kinetics. Deviations from this case lead to complications in the signal's interpretation. Samoc and Prasad [7] first reported that the high-order kinetic equations led to an uneven reduction of the grating pattern and the appearance of new Fourier components. Vauthey [9] argued that in order to measure accurately the population of photoproducts via TG, the FDO alone is not sufficient.

To understand the origin of the FDO and SDO time evolution in our case, we simulated the grating's temporal evolution of the charge carrier kinetics according to the rate equation (1). The  $D$ ,  $k_1$ ,  $k_2$  and  $k_3$  coefficients are known for valence excitation [20, 35, 36], but the EUV excitation (pre- or post-edge) creates charge carriers with widely different kinetic energy distributions, whose behavior cannot be described using the coefficients for valence excitation. The time scale of relevance where these coefficients are operative is limited to 10 ps. Under these conditions,  $k_1$  and  $k_2$  can be neglected because the complete recovery of the system occurs on nsec time scales (cf Weagele *et al* [20] as well as figure S3). As argued by Bohinc *et al* [16], and confirmed by previous measurement of diffusion coefficients [37], the diffusion time is also not relevant on the sub-10 ps time scale and therefore, the kinetics are dominated by IAR, captured by the three-body bulk recombination rate  $k_3$ . Here, we used a value of  $3 \cdot 10^{-31} \text{ cm}^{-6} \text{ s}^{-1}$  to best reproduce the grating's behavior. Just as in the experiment, in the model we increase the contribution of the IAR component of equation (1) by maintaining the FEL power constant while tuning  $E_{\text{exc}}$  across the Co  $M_{2,3}$  edge. The initial carrier density is then scaled according to the computed sample absorption. The gratings are propagated by solving equation (1) for each initial condition. We added a Gaussian function with a 150 fs standard deviation to simulate the cross-correlation of the instrument, and a constant contribution via a Heaviside function convoluted with the instrument response in order to capture the dynamics at longer timescales.

Under our experimental conditions, the sample thickness is small compared to the grating pitch and we can use the thin grating approximation where the TG pattern modulates the complex index of refraction of the sample. This modulation

can be decomposed into Fourier coefficients, whose square values are directly linked to the diffraction order intensities [7]. The computed FDO and SDO traces are shown in figure 3 along with the experimental data (dots) for low and high initial carrier densities, respectively. They capture the main features of the traces, i.e. the time zero signal and the grating evolution. In particular, they capture the drastic difference between FDO and SDO profiles and, for the latter, their changes as a function of carrier density. Some deviations also show up, in particular in the SDO, where the long-time response exhibits a double structure at 64 eV with a maximum at 3 ps and another one at 8 ps. However, this double feature does not seem to occur at 59 and 61 eV (figure 2), and more systematic studies would be needed to confirm or invalidate it.

To understand the differences between FDO and SDO traces, we need to consider the time evolution of the grating's Fourier components. The initial photo-induced grating of electronic excitations contains a single Fourier component following the interference of the FEL-beams. Considering only first order kinetics in equation (1), the system's temporal evolution would conserve such a single Fourier component and the evolution of the FDO would directly reflect the charge carrier lifetimes and diffusion [5]. This is the dominant contribution to the traces obtained for small charge carrier densities (e.g. FDO and SDO traces at 57 eV in figure 3). This behavior fails when the light-matter interaction ventures away from the linear interaction as in the case of two-photon absorption, saturated absorption or when the system's evolution follows second or higher-order kinetics [7]. In this later case, the carrier decay rate depends on the local carrier density and varies across the grating. This yields to an increased flattening of its pattern with the appearance of higher order Fourier components, leading to the marked changes in the SDO traces as a function of the photon energy and, thus, carrier density. We would expect a similar behavior at fixed FEL photon energy and by tuning of the pulse energy.

The dominant mechanisms at the highest carrier densities are attributed to the three-body process of IAR. The evolution from sinusoidal to non-sinusoidal gratings can be seen in figures 4(a) and (b), where we show the grating patterns at different time delays and excitation conditions. In figure 4(a), we show the time evolution of the grating corresponding to a high initial carrier density of  $6.4 \times 10^{20} \text{ cm}^{-3}$ . The initial sinusoidal grating displayed as a dotted line is harmonic but as the dynamics evolve, a clear flattening of the pattern is observed and is responsible for the delayed increase of the SDO intensity. In figure 4(b), the flattening of two gratings at 10 ps time delay are compared with the initial sinusoidal grating. The two flattened gratings correspond to the situation with initial carrier densities of  $2.5 \times 10^{20} \text{ cm}^{-3}$  and  $6.4 \times 10^{20} \text{ cm}^{-3}$ , respectively. Here, the principal variation at the two excitation energies in the grating pattern is their periodicities. The grating periodicity affects the phase matched emission angle but has a negligible effect on the kinetics at these time delay and therefore, this cannot explain the time evolution of the SDO. The latter is instead dictated by the small variation of the grating pattern in regions of high carrier densities at the grating

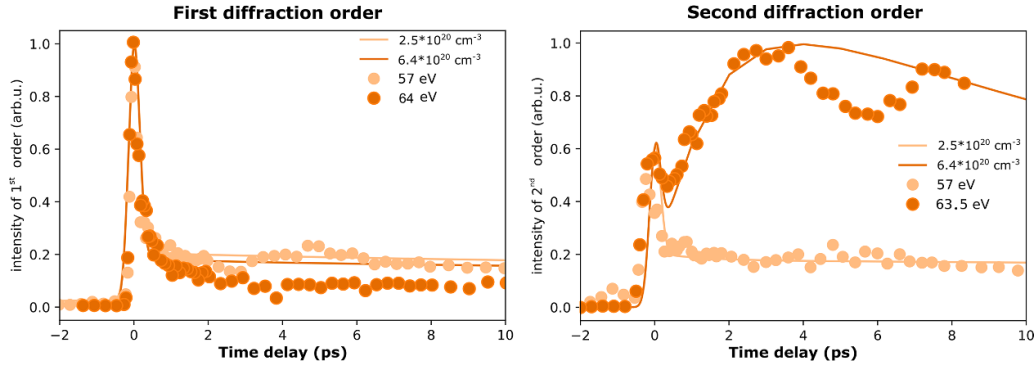


**Figure 3.** The dots represent the experimental FDO and SDO traces recorded at incident energies below (57 eV) and above (64 eV) the Co  $M_{2,3}$ -edge. The solid lines are simulations of the grating time evolution using equation (1).

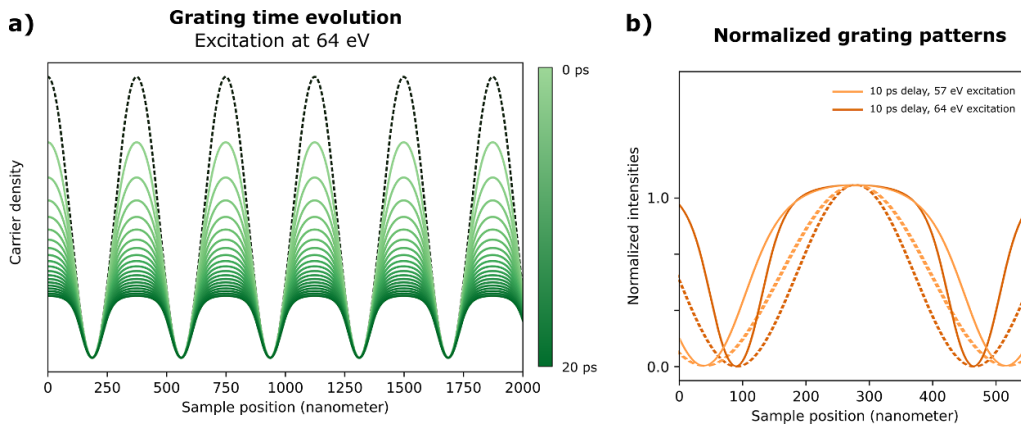


**Figure 4.** (a) Spatial modulation of the carrier density between 0 and 20 ps in steps of 1 ps following excitation at 64 eV. The initial grating pattern is shown as a dotted line. (b) Full lines are the calculated gratings at 10 ps time delay after excitations below and above the cobalt  $M_{2,3}$  edge (i.e. 57 and 64 eV, respectively). These two non-sinusoidal gratings are compared to the sinusoidal gratings (dashed lines) present at time zero.

maxima. These changes in grating shapes amount to only a few nanometres but are responsible for the large shape variations between the FDO and SDO time traces (unfortunately, a direct comparison of FDO to SDO intensities is not possible due to drifts in the spatial overlap when switching between diffraction orders). This highlights the high spatial sensitivity of TG spectroscopy resolved on the FDO and SDO traces.

#### 4. Conclusion

We have carried out EUV-TG experiments of the spinel  $\text{Co}_3\text{O}_4$  compound at various initial carrier densities by tuning  $E_{\text{exc}}$  from 57 to 64 eV across the Co  $M_{2,3}$ -edge, probing the first and second order diffraction of a 395 nm pulse. The observed behavior is attributed to the increased carrier density, resulting into an increasing weight of high order kinetic terms in the master kinetic rate equation, which triggers the appearance of high-order Fourier components in the grating pattern. We thus conclude that the evolution from a sinusoidal to a non-sinusoidal grating is due to processes that follow the third order kinetic terms of the population relaxation, which can hereby be probed thanks to the extreme sensitivity of the SOD signal to high order kinetics.

The study of condensed matter systems following EUV excitation is highly complex as the large amount of energy deposited by the energetic photons brings the system far away from its ground state behavior. Here, we demonstrate that EUV TG resolved on multiple diffraction orders provides not only spectroscopic information on the kinetics but also clear insights on the order term of the kinetics equations at play. Going to even higher orders (e.g. third order) [38] is in principle possible. It may more precisely harness the evolution of the grating. However, to our knowledge no such measurements have so far been reported in the optical domain. In the EUV domain, the phase matching conditions are not favorable using an optical probe, but it is an open question for TG experiments using EUV probe pulses.

#### 5. Methods

Using the mini-TIMER set-up, two FEL pulses are crossed at  $2\theta = 2.7^\circ$  on a 27 nm-thick  $\text{Co}_3\text{O}_4$  sample deposited on a sapphire substrate at room temperature. The 395 nm probe beam is incident on the sample at an angle of  $45^\circ$ . The FEL FERMI with values of  $E_{\text{exc}}$  ranging from 55 to 70 eV, generating TG's

with values of  $L_{TG}$  from 478 to 376 nm, respectively [39]. FDO and SDO signals are recorded in three consecutive scans with similar FEL conditions (i.e. power, photon energy etc), and then averaged. A direct comparison of FDO to SDO intensities is not possible due to drifts in the spatial overlap when switching between diffraction orders. The camera background is collected and subtracted by blocking the FEL beam at the beginning of each scan. After each scan, we ensured that no permanent grating is formed on the sample by checking that no diffracted beam is detected with the 395 nm pulse alone. The  $\theta = 45^\circ$  incidence angle between the FEL and the probe beam leads to smearing of the temporal resolution that also depends on the relative laser spot sizes. Considering a focus size of  $\sigma = 100 \mu\text{m}$  for the optical laser, this leads to an upper limit on the temporal resolution of  $(\sigma \cdot \tan\theta)/c \approx 300$  fs, which is negligible compared to the temporal evolution monitored in this work.

Figure S1 shows the computed absorption spectrum of a 27 nm thick spinel  $\text{Co}_3\text{O}_4$  sample along with the element's contributions [40]. Excitation in the vicinity of the cobalt  $M_{2,3}$ -edge implies non-negligible absorption by the tail of the oxygen valence ionization continuum whose edge peaks at 20 eV. In order to ensure the stability of the FEL radiation, the current created by the EUV pulses on an up-stream mirror from the experiment is recorded. This  $I_0$  value is shown in figure S2 for the various scans.

### Data availability statement

All data that support the findings of this study are included within the article (and any supplementary files).

### Acknowledgments

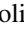
This work was supported by the ERC Advanced Grants DYNAMOX (695197), and the French–German–Swiss Solar Nitrogen Fixation: Ammonia from Sunlight and Air (FN n°20SC-1\_187032), and the swiss NSF via the NCCR:MUST. HJBM acknowledges support by the ERC starting grant SATTOC (101078595). G F M acknowledges support from ERC Starting Grant ULTRAIMAGE (851154), ERC PoC HYPER (101123123). M C acknowledges support from the ERC Advanced Grant CHIRAX (101095012).

### ORCID iDs

Oliviero Cannelli  <https://orcid.org/0000-0002-1844-4799>

Rebecca A Ingle  <https://orcid.org/0000-0002-0566-3407>

Romain Geneaux  <https://orcid.org/0000-0002-3395-6813>

Emanuele Pedersoli  <https://orcid.org/0000-0003-0572-6735>

Filippo Bencivenga  <https://orcid.org/0000-0003-3929-5101>

Majed Chergui  <https://orcid.org/0000-0002-4856-226X>

### References

- [1] Ramer A, Osmani O and Rethfeld B 2014 Laser damage in silicon: energy absorption, relaxation, and transport *J. Appl. Phys.* **116** 53508
- [2] van Driel H M 1987 Kinetics of high-density plasmas generated in Si by 1.06- and 0.53  $\mu\text{m}$  picosecond laser pulses *Phys. Rev. B* **35** 8166–76
- [3] Salcedo J R, Siegman A E, Dlott D D and Fayer M D 1978 Dynamics of energy transport in molecular crystals: the picosecond transient-grating method *Phys. Rev. Lett.* **41** 131–4
- [4] Arias D H, Moore D T, van de Lagemaat J and Johnson J C 2018 Direct measurements of carrier transport in polycrystalline methylammonium lead iodide perovskite films with transient grating spectroscopy *J. Phys. Chem. Lett.* **9** 5710–7
- [5] Fayer M D 1982 Dynamics of molecules in condensed phases: picosecond holographic grating experiments *Annu. Rev. Phys. Chem.* **33** 63–87
- [6] Mukamel S 1995 *Principles of Nonlinear Optical Spectroscopy* (Oxford University Press)
- [7] Samoc M and Prasad P N 1989 Dynamics of resonant third-order optical nonlinearity in perylene tetracarboxylic dianhydride studied by monitoring first- and second-order diffractions in subpicosecond degenerate four-wave mixing *J. Chem. Phys.* **91** 6643–9
- [8] Asahi T, Tamai N, Uchida T, Shimo N and Masuhara H 1995 Nonlinear excited-state dynamics of a thin copper phthalocyanine film by femtosecond transient grating spectroscopy *Chem. Phys. Lett.* **234** 337–42
- [9] Vauthey E 1997 Applicability of the transient grating technique to the investigation of photoinduced processes following second order kinetics *J. Photochem. Photobiol. A* **109** 195–200
- [10] Bencivenga F, Baroni S, Carbone C, Chergui M, Danaïlov M B, De Ninno G, Kiskinova M, Raimondi L, Svetina C and Masciovecchio C 2013 Nanoscale dynamics by short-wavelength four wave mixing experiments *New J. Phys.* **15** 123023
- [11] Chergui M, Beye M, Mukamel S, Svetina C and Masciovecchio C 2023 Progress and prospects in nonlinear extreme-ultraviolet and x-ray optics and spectroscopy *Nat. Rev. Phys.* **5** 578–96
- [12] Bencivenga F 2015 Four-wave mixing experiments with extreme ultraviolet transient gratings *Nature* **520** 205–8
- [13] Bencivenga F *et al* 2019 Nanoscale transient gratings excited and probed by extreme ultraviolet femtosecond pulses *Sci. Adv.* **5** eaaw5805
- [14] Maznev A A *et al* 2018 Generation of coherent phonons by coherent extreme ultraviolet radiation in a transient grating experiment *Appl. Phys. Lett.* **113** 221905
- [15] Maznev A A *et al* 2021 Generation and detection of 50 GHz surface acoustic waves by extreme ultraviolet pulses *Appl. Phys. Lett.* **119** 44102
- [16] Bohinc R *et al* 2019 Nonlinear XUV-optical transient grating spectroscopy at the Si  $L_{2,3}$ -edge *Appl. Phys. Lett.* **114** 181101
- [17] Ksenzov D *et al* 2021 Nanoscale transient magnetization gratings created and probed by femtosecond extreme ultraviolet pulses *Nano Lett.* **21** 2905–11
- [18] Rouxel J R *et al* 2021 Hard x-ray transient grating spectroscopy on bismuth germanate *Nat. Photon.* **15** 499–503
- [19] Yao K *et al* 2022 All-optical switching on the nanometer scale excited and probed with femtosecond extreme ultraviolet pulses *Nano Lett.* **22** 4452–8



- [20] Waegele M M, Doan H Q and Cuk T 2014 Long-lived photoexcited carrier dynamics of d–d excitations in spinel ordered  $\text{Co}_3\text{O}_4$  *J. Phys. Chem. C* **118** 3426–32
- [21] Jiang C-M *et al* 2014 Characterization of photo-induced charge transfer and hot carrier relaxation pathways in spinel cobalt oxide ( $\text{Co}_3\text{O}_4$ ) *J. Phys. Chem. C* **118** 22774–84
- [22] Biswas S, Husek J, Londo S and Baker L R 2018 Highly localized charge transfer excitons in metal oxide semiconductors *Nano Lett.* **18** 1228–33
- [23] Zhang Y, Zhang C, Huang X, Yang Z, Zhang K H L and Yang Y 2021 Barrierless self-trapping of photocarriers in  $\text{Co}_3\text{O}_4$  *J. Phys. Chem. Lett.* **12** 12033–9
- [24] Allaria E *et al* 2012 Highly coherent and stable pulses from the FERMI seeded free-electron laser in the extreme ultraviolet *Nat. Photon.* **6** 699–704
- [25] De Ninno G, Mahieu B, Allaria E, Giannessi L and Spampinati S 2013 Chirped seeded free-electron lasers: self-standing light sources for two-color pump-probe experiments *Phys. Rev. Lett.* **110** 64801
- [26] Klebanoff L E, Van Campen D G and Pouliot R J 1994 Spin-resolved and high-energy-resolution XPS studies of cobalt metal and a cobalt magnetic glass *Phys. Rev. B* **49** 2047–57
- [27] Othonos A 1998 Probing ultrafast carrier and phonon dynamics in semiconductors *J. Appl. Phys.* **83** 1789–830
- [28] Cushing S K *et al* 2018 Hot phonon and carrier relaxation in Si(100) determined by transient extreme ultraviolet spectroscopy *Struct. Dyn.* **5** 54302
- [29] Baldini E, Palmieri T, Pomarico E, Auböck G and Chergui M 2018 Clocking the ultrafast electron cooling in anatase titanium dioxide nanoparticles *ACS Photonics* **5** 1241–9
- [30] Medvedev N and Rethfeld B 2010 Transient dynamics of the electronic subsystem of semiconductors irradiated with an ultrashort vacuum ultraviolet laser pulse *New J. Phys.* **12** 73037
- [31] Sambur J B, Novet T and Parkinson B A 2010 Multiple exciton collection in a sensitized photovoltaic system *Science* **330** 63–66
- [32] Boubanga-Tombet S, Wright J B, Lu P, Williams M R C, Li C, Wang G T and Prasankumar R P 2016 Ultrafast carrier capture and auger recombination in single GaN/InGaN multiple quantum well nanowires *ACS Photonics* **3** 2237–42
- [33] Vaxenburg R, Rodina A, Shabaev A, Lifshitz E and Efros A L 2015 Nonradiative auger recombination in semiconductor nanocrystals *Nano Lett.* **15** 2092–8
- [34] Haug A 1983 Auger recombination in direct-gap semiconductors: band-structure effects *J. Phys. C* **16** 4159–72
- [35] Büttner G *et al* 2017 Thermoelectric properties of  $[\text{Ca}_2\text{CoO}_{3-\delta}][\text{CoO}_2]_{1.62}$  as a function of Co/Ca defects and  $\text{Co}_3\text{O}_4$  inclusions *J. Appl. Phys.* **121** 215101
- [36] Patil V, Joshi P, Chougule M and Sen S 2012 Synthesis and characterization of  $\text{Co}_3\text{O}_4$  thin film *Soft Nanosci. Lett.* **2** 16574
- [37] Baker L R, Jiang C-M, Kelly S T, Lucas J M, Vura-Weis J, Gilles M K, Alivisatos A P and Leone S R 2014 Charge carrier dynamics of photoexcited  $\text{Co}_3\text{O}_4$  in methanol: extending high harmonic transient absorption spectroscopy to liquid environments *Nano Lett.* **14** 5883–90
- [38] Weder D *et al* 2020 Transient magnetic gratings on the nanometer scale *Struct. Dyn.* **7** 054501
- [39] Bencivenga F *et al* 2016 Experimental setups for FEL-based four-wave mixing experiments at FERMI *J. Synchrotron Radiat.* **23** 132–40
- [40] Henke B L, Gullikson E M and Davis J C 1993 X-ray interactions: photoabsorption, scattering, transmission, and reflection at  $E = 50\text{--}30,000$  eV,  $Z = 1\text{--}92$  *At. Data Nucl. Data Tables* **54** 181–342